symmetry

MDPI

Article

Numerical Solutions of the Mathematical Models on the Digestive System and COVID-19 Pandemic by Hermite Wavelet Technique

Kumbinarasaiah Srinivasa [1], Haci Mehmet Baskonus [2] and Yolanda Guerrero Sánchez [3,*]

[1] Department of Mathematics, Bangalore University, Bengaluru, Karnataka 560056, India; kumbinarasaiah@gmail.com
[2] Faculty of Education, Harran University, Sanliurfa 63050, Turkey; hmbaskonus@gmail.com
[3] Departamento de Anatomía y Psicobiología, Universidad de Murcia, 30001 Murcia, Spain
* Correspondence: yolanda.guerreros@um.es

Abstract: This article developed a functional integration matrix via the Hermite wavelets and proposed a novel technique called the Hermite wavelet collocation method (HWM). Here, we studied two models: the coupled system of an ordinary differential equation (ODE) is modeled on the digestive system by considering different parameters such as sleep factor, tension, food rate, death rate, and medicine. Here, we discussed how these parameters influence the digestive system and showed them through figures and tables. Another fractional model is used on the COVID-19 pandemic. This model is defined by a system of fractional-ODEs including five variables, called S (susceptible), E (exposed), I (infected), Q (quarantined), and R (recovered). The proposed wavelet technique investigates these two models. Here, we express the modeled equation in terms of the Hermite wavelets along with the collocation scheme. Then, using the properties of wavelets, we convert the modeled equation into a system of algebraic equations. We use the Newton–Raphson method to solve these nonlinear algebraic equations. The obtained results are compared with numerical solutions and the Runge–Kutta method (R–K method), which is expressed through tables and graphs. The HWM computational time (consumes less time) is better than that of the R–K method.

Keywords: differential equations; operational matrix of integration; collocation method; Hermite wavelets

Citation: Srinivasa, K.; Baskonus, H.M.; Guerrero Sánchez, Y. Numerical Solutions of the Mathematical Models on the Digestive System and COVID-19 Pandemic by Hermite Wavelet Technique. *Symmetry* **2021**, *13*, 2428. https://doi.org/10.3390/sym13122428

Academic Editor: José Carlos R. Alcantud

Received: 9 November 2021
Accepted: 12 December 2021
Published: 15 December 2021

1. Introduction

Recently, with the help of newly developed computational methods, many experts extracted more deep features of real world problems such as symmetry, optical waves, gravitational potentials and so on. Experts extracted the symmetrical properties of such models by using mathematical norms. Thus, many experts developed some new operators and models. So, the coupled ordinary differential equations (ODEs) of integer and fractional order are used to describe many physical phenomena in symmetry, physics, fluid dynamics, mathematical biology, and bio-modeling. Many experts have considered these models over hundreds of years, and there are many well-developed solution procedures. Often, some models described by ODEs are so complex that a purely analytical solution to such equations is not tractable. For those sorts of complex models, numerical methods are helpful. When the analytical solution is not possible, then switching over to the numerical method is preferred. As a result, we proposed a novel approach called HWM to solve the system of coupled ODEs. The primary purpose is to present and explain a new numerical method for obtaining the approximate solution to the system of coupled equations of integer and fractional orders that cannot be solved exactly.

Wavelet theory is one of the recent emerging approaches in applied mathematics. It has a wide range of applications in the following fields as signal analyses, computer

science, mathematical modeling, image processing, and applied sciences. Many mathematicians' contributions toward wavelets-based numerical methods and fractional models are as follows: the Laguerre wavelets method for the Lane–Emden equation [1], Hermite wavelets method [2,3], Laguerre wavelets collocation method [4,5], numerical solution of some biological models [6–10], and numerical approach for fractional models [11–24], etc. According to the current literature survey, HWM is used to solve ODE, PDE, fractional ODE, and fractional PDEs. Still, mathematical models on the digestive system and fractional models on the COVID-19 pandemic have not been studied by any mathematicians using the wavelet technique. Using the information with the vaccination, experts may observe more profound properties of the vaccination by using mathematical tools that are guaranteed scientifically. This impels us to solve such equations via the Hermite wavelets method (HWM). The interest of the present work is to solve the system of ODEs for both integer and fractional order by using the HWM, and the obtained results are compared with the results of the numerical method.

A variety of exact, approximate and purely numerical methods are available to solve the system of ODEs. Most of these methods are computationally rigorous because they are trial-and-error in character or need complex computations. Some problems are often solved by the system of ordinary differential equations in reality, such as in modern physics, engineering, etc. Anticipating the exact solution for such equations is rigorous. So, it is necessary to use a numerical method to solve such a problem. This paper mainly used the R–K method and HWM to solve the integer and fractional order ODE system. Consider that the mathematical model on the digestive system is of the form [7]:

$$\left.\begin{array}{ll} \frac{dT(x)}{dx} = -\alpha F(x) - \beta & T(0) = A \\ \frac{dF(x)}{dx} = \delta T(x) + \gamma M(x) & F(0) = B \\ \frac{dM(x)}{dx} = -\delta T(x) + \beta M(x) - d & M(0) = C \end{array}\right\} \tag{1}$$

where α represents the quantity of food, and the minus sign indicates the smaller amount of food. β shows the sleep factor, δ is used for the tension rate, γ denotes the recovery term, and d shows the death rate. Moreover, $T(0) = A$, $F(0) = B$, $M(0) = C$ are the initial conditions for all compartments of the given model. We considered four different cases to analyze the given model and solved it by the R–K method and HWM. Here, $T(x)$, $F(x)$, $M(x)$ stands for tension, food, and medicine, respectively. We study to observe the numerical and symmetrical wave propagations of Equation (1) in graphs and tables. Another important fractional system of ODEs for the COVID-19 pandemic model [11] given as:

$$\left.\begin{array}{ll} {}_0^cD_x^\delta S = \wedge^\delta - \mu^\delta S - \beta^\delta S(E+I) & S(0) = 153 \\ {}_0^cD_x^\delta E = \beta^\delta S(E+I) - \pi^\delta E - (\mu^\delta + \gamma^\delta)E & E(0) = 55 \\ {}_0^cD_x^\delta I = \pi^\delta E - \sigma^\delta I - \mu^\delta I & I(0) = 79 \\ {}_0^cD_x^\delta Q = \gamma^\delta E + \sigma^\delta I - (\theta^\delta + \mu^\delta)Q & Q(0) = 68 \\ {}_0^cD_x^\delta R = \theta^\delta Q - \mu^\delta R & R(0) = 20 \end{array}\right\} \tag{2}$$

where $0 < \delta < 1$, and ${}_0^cD_x^\delta$ denotes the fractional derivative in the Caputo sense. S, E, I, Q, R represent the susceptible, exposed, infected, isolated, and recovered population, respectively. $\Lambda = \mu N$ is recruitment rate, β is the rate at which those susceptible become infected and exposed, π is the rate at which the exposed population become infected, γ is the rate at which exposed people become isolated, σ is the rate at which infected people are added to isolated individuals, θ is the rate at which isolated persons become recovered, μ is the natural death rate and disease-related death rate. We solved this problem for different fractional-order and compared the HWM solution with the R–K method solution.

The R–K method is a well-known and universally accepted method. The main advantages of Runge–Kutta methods are that they are easy to implement, and they are very stable. The Hermite wavelet method is a new method, and here, we showed that it can be used to solve the biological models for both integer and fractional ordered coupled ODEs.

The primary disadvantages of Runge–Kutta methods are that they require significantly more computer time than multi-step methods of comparable accuracy, and they do not easily yield good global estimates of the truncation error. However, this cannot happen with the Hermite wavelet method. For the particular domain, we get the solution with less computation time. As a result, the Hermite wavelet method is better than the R–K method. Therefore, we used these two methods in this article.

This paper's organization is as follows: Section 2 is devoted to the progress of the Hermite wavelet operational matrix of integration, function approximation, and theorems on convergence analysis. Section 3 reveals the method of solution. In Section 4, we present the application of the HWM to the governing model. By using projected method, we observe the symmetrical and wave features of the governing models. In Section 5, we present some important results and discussion. Finally, this paper is completed by giving critical new findings in conclusion in Section 6.

2. Hermite Wavelet Operation Matrix of Integration, the Definition of Fractional Derivatives, and Some Results on Convergence Analysis

Definition 1. *The Riemann–Liouville's fractional integral of $f \epsilon C_\mu$ of the order $\delta \geq 0$ is defined as [15]*

$$J_s^\delta f(s) = \begin{cases} f(s) & if\ \delta = 0 \\ \frac{1}{\Gamma(\delta)} \int_0^s (s-t)^{\delta-1} f(t) dt & if\ \delta > 0. \end{cases}$$

Here, Γ denotes the gamma function.

Definition 2. *The Caputo fractional derivative of $f(s)\ \epsilon\ C_\mu$ is defined as [15]:*

$$\frac{\partial^\delta f(s)}{\partial s^\delta} = \frac{1}{\Gamma(m-\delta)} \int_0^s (s-t)^{m-\delta-1} f^{(m)}(t)\ dt$$

for $m-1 < \delta \leq m$, m is any positive integer, $s > 0$, $f(s) \epsilon {C_\mu}^m$, $\mu \geq -1$.

The Hermite wavelet is one of the continuous polynomial basis wavelets studied in [4]. Now, we approximate the solution $y(x)$ of the nonlinear differential equation under the Hermite wavelet space as follows:

$$y(x) = \sum_{n=1}^{\infty} \sum_{m=0}^{\infty} C_{n,m} \varphi_{n,m}(x), \tag{3}$$

where $\varphi_{n,m}(x)$ is given in [4]. We approximate $y(x)$ by truncating the series as follows

$$y(x) \approx \sum_{n=1}^{2^{k-1}} \sum_{m=0}^{M-1} C_{n,m} \varphi_{n,m}(x) = A^T \varphi(x), \tag{4}$$

where A and $\varphi(x)$ are $2^{k-1}M \times 1$ matrix,

$$A^T = [C_{1,0}, \ldots C_{1,M-1}, C_{2,0} \ldots C_{2,M-1}, \ldots C_{2^{k-1},0}, \ldots C_{2^{k-1},M-1}],$$

$$\varphi(x) = [\varphi_{1,0}, \ldots \varphi_{1,M-1}, \varphi_{2,0}, \ldots \varphi_{2,M-1}, \ldots \varphi_{2^{k-1},0}, \ldots \varphi_{2^{k-1},M-1}]^T.$$

Let $\{\phi_{i,j}\}$ be the sequence of Hermite wavelets, n = 1, 2, ... and m = 0, 1, ... For every fixed n, there is a Hermite space spanned by the elements of the sequence $\{\phi_{i,j}\}$. That is, $L(\{\phi_{i,j}\}) = H^2[0,1)$ is Banach space.

Theorem 1 ([17]). *Let $\{\phi_{i,j}(t)\}$ be the sequence of Hermite wavelets in $C([a,\ b])$ in t on $[a,\ b]$ converges to the function $\phi(t)$ in $C([a,\ b])$ uniformly in t on $[a,\ b]$. Then, $\phi(t)$ is continuous in $C([a,\ b])$ in t on $[a,\ b]$.*

Theorem 2 ([19]). *A continuous function $y(x)$ in $H^2[0,1)$ defined on $[0,1)$ be bounded; then, the Hermite wavelets expansion of $y(x)$ converges to it.*

Theorem 3 ([4]). *Suppose that $y(x) = C^m[0,1]$ and $C^T\phi(x)$ is the approximate solutionusing Hermite wavelets. Then, the error bound would be given by*

$$\| E(x) \| \leq \| \frac{2}{m! 4^m 2^{m(k-1)}} \max_{x \in [0,1]} |y^m(x)| \| .$$

Theorem 4 ([16]). *Let $(S(0), E(0), I(0), Q(0))$ be any initial data belonging to R_+^4 and $(S(x), E(x), I(x), Q(x))$ be the solution corresponding to the initial data. Then, the set R_+^4 is a positively invariant set of the model. Furthermore, we have*

$$\limsup_{x \to \infty} S(x) \leq S_\infty = \frac{\wedge^\delta}{\mu^\delta},$$

$$\limsup_{x \to \infty} E(x) \leq E_\infty = \frac{\wedge^\delta}{\pi^\delta + \mu^\delta + \gamma^\delta},$$

$$\limsup_{x \to \infty} I(x) \leq I_\infty = \frac{\pi^\delta E_\infty}{\sigma^\delta + \mu^\delta},$$

$$\limsup_{x \to \infty} Q(x) \leq Q_\infty = \frac{\gamma^\delta E_\infty + \sigma^\delta I_\infty}{\mu^\delta + \alpha^\delta},$$

$$\limsup_{x \to \infty} R(x) \leq \frac{\theta^\delta}{\mu^\delta}.$$

Theorem 5 ([19]). *Suppose $y \in C^p[0,1)$ is an p times continuously differentiable function such that $y = \sum_{n=1}^{2^{k-1}} y_n(x)$ and $\{\phi_{n,m}\}$ be a sequence of Hermite wavelets, where $n = 1, \ldots, 2^{k-1}$ and $m = 0, \ldots, M-1$, k is any positive integer. Let $Y_n = L(\{\varphi_{\mathrm{n.m}}\})$ be the linear space spanned by $\{\phi_{n,m}\}$. If $C_n^T H_n(x)$ is the best approximation to y_n, then $C^T H(x)$ approximates y with the following error bound:*

$$||y - C^T H(x)||_2 \leq \frac{k}{\sqrt{(2p+1)} 2^{(k-1)(p+\frac{1}{2})}}, \; K = \max y^p(\xi), \; \forall \, \xi \in [\frac{n-1}{2^{k-1}}, \frac{n}{2^{k-1}}).$$

Operational Matrix of Integration

Hermite wavelet: Wavelets constitute a family of functions constructed from the dilation and translation of a single function called the mother wavelet. When the dilation parameter a and translation parameter b vary continuously, we have the following family of continuous wavelets:

$$\varphi_{a,b}(x) = |a|^{-1/2} \varphi\left(\frac{x-b}{a}\right), \forall a, b \in R, \, a \neq 0.$$

If we restrict the parameters a and b to discrete values as $a = a_0^{-k}$, $b = n b_0 a_0^{-k}$, $a_0 > 1$, $b_0 > 0$, we have the following family of discrete wavelets: $\varphi_{k,n}(x) = |a|^{1/2} \varphi(a_0^k x - n b_0)$, $\forall a, b \in R$, $a \neq 0$, where $\varphi_{k,n}$ form a wavelet basis for $L^2(R)$. In particular, when $a_0 = 2$ and $b_0 = 1$, then $\varphi_{k,n}(x)$ forms an orthonormal basis. Hermite wavelets are defined as,

$$\varphi_{n,m}(x) = \begin{cases} \frac{2^{\frac{k+1}{2}}}{\sqrt{\pi}} h_m(2^k x - 2n + 1), & \frac{n-1}{2^{k-1}} \leq x < \frac{n}{2^{k-1}}, \\ 0, & \text{otherwise.} \end{cases}$$

where $m = 0, 1, \ldots, M-1$ and $n = 1, 2, \ldots, 2^{k-1}$, k is assumed as any positive integer. Here, $h_m(x)$ are the Hermite polynomials of degree m concerning the weight function $W(x) = \sqrt{1-x^2}$ on the real line R and satisfy the following recurrence formula,

$$h_0(x) = 1, \;\; h_1(x) = 2x, \;\; h_{m+2}(x) = 2xh_{m+1}(x) - 2(m+1)h_m(x),$$

where $m = 0, 1, 2, \ldots$

Consider six Hermite wavelet bases at $k = 1$ and $M = 6 = N$; then, we get

$$\begin{aligned}
\varphi_{1,0}(x) &= \tfrac{2}{\sqrt{\pi}} \\
\varphi_{1,1}(x) &= \tfrac{1}{\sqrt{\pi}}(8x-4) \\
\varphi_{1,2}(x) &= \tfrac{1}{\sqrt{\pi}}(32x^2-32x+4) \\
\varphi_{1,3}(x) &= \tfrac{1}{\sqrt{\pi}}(128x^3-192x^2+48x+8) \\
\varphi_{1,4}(x) &= \tfrac{1}{\sqrt{\pi}}(512x^4-1024x^3+384x^2+128x-40) \\
\varphi_{1,5}(x) &= \tfrac{1}{\sqrt{\pi}}(2048x^5-5120x^2+2560x^3+1280x^2-800x+16)
\end{aligned}$$

where

$$\varphi(x) = [\varphi_{1,0}(x), \varphi_{1,1}(x), \varphi_{1,2}(x)\varphi_{1,3}(x)\varphi_{1,4}(x)\varphi_{1,5}(x)].$$

Now, integrate the above basis concerning x limit from 0 to x; then, express as a linear combination of Hermite wavelet basis as

$$\begin{aligned}
\int_0^x \phi_{1,0}(x) &= \left[\begin{array}{cccccc} \frac{1}{2} & \frac{1}{4} & 0 & 0 & 0 & 0 \end{array}\right] \phi_6(x) \\
\int_0^x \phi_{1,1}(x) &= \left[\begin{array}{cccccc} \frac{-1}{4} & 0 & \frac{1}{8} & 0 & 0 & 0 \end{array}\right] \phi_6(x) \\
\int_0^x \phi_{1,2}(x) &= \left[\begin{array}{cccccc} \frac{-1}{3} & 0 & 0 & \frac{1}{12} & 0 & 0 \end{array}\right] \phi_6(x) \\
\int_0^x \phi_{1,3}(x) &= \left[\begin{array}{cccccc} \frac{5}{4} & 0 & 0 & 0 & \frac{1}{16} & 0 \end{array}\right] \phi_6(x) \\
\int_0^x \phi_{1,4}(x) &= \left[\begin{array}{cccccc} \frac{-2}{5} & 0 & 0 & 0 & 0 & \frac{1}{12} \end{array}\right] \phi_6(x) \\
\int_0^x \phi_{1,5}(x) &= \left[\begin{array}{cccccc} \frac{-23}{3} & 0 & 0 & 0 & 0 & 0 \end{array}\right] \phi_6(x) + \tfrac{1}{24}\overline{\phi_{1,6}}(x).
\end{aligned}$$

Therefore,

$$\int_0^x \phi(x)dx = P_{6\times 6}\phi_6(x) + \overline{\phi_6}(x)$$

where

$$P_{6\times 6} = \begin{bmatrix} \frac{1}{2} & \frac{1}{4} & 0 & 0 & 0 & 0 \\ \frac{-1}{4} & 0 & \frac{1}{8} & 0 & 0 & 0 \\ \frac{-1}{3} & 0 & 0 & \frac{1}{12} & 0 & 0 \\ \frac{5}{4} & 0 & 0 & 0 & \frac{1}{16} & 0 \\ \frac{-2}{5} & 0 & 0 & 0 & 0 & \frac{1}{20} \\ \frac{-23}{3} & 0 & 0 & 0 & 0 & 0 \end{bmatrix}, \; \overline{\varphi_6}(x) = \begin{bmatrix} 0 \\ 0 \\ 0 \\ 0 \\ 0 \\ \frac{1}{24}\overline{\varphi_{1,6}}(x) \end{bmatrix}.$$

3. Hermite Wavelets Method

Here, we would like to express the solution of a system of ODE in terms of Hermite wavelets.

3.1. Hermite Wavelets Method for Digestive Model

Assume that

$$T' = A^T\phi(x). \tag{5}$$

Integrate Equation (5) concerning x, limit from 0 to x, we get

$$T = T(0) + A^T[P\phi(x) + \overline{\phi(x)}]$$

$$T = 0.9999 + A^T[P\phi(x) + \overline{\phi(x)}]. \tag{6}$$

Again, assume

$$F' = B^T\phi(x). \tag{7}$$

Integrate Equation (7) concerning x, limit from 0 to x, we get

$$F = F(0) + B^T[P\phi(x) + \overline{\phi(x)}]$$

$$F = 0.0001 + B^T[P\phi(x) + \overline{\phi(x)}]. \tag{8}$$

Again, choose

$$M' = C^T\phi(x). \tag{9}$$

Integrate Equation (9) concerning x, limit from 0 to x.

$$M = M(0) + C^T[P\phi(x) + \overline{\phi(x)}]$$

$$M = C^T[P\phi(x) + \overline{\phi(x)}] \tag{10}$$

Now, substitute (5) to (10) in (1); then, we get

$$A^T\phi(x) = -\alpha[0.001 + B^T\left[P\phi(x) + \overline{\phi(x)}\right] - \beta$$

$$B^T\phi(x) = \delta[0.9999 + A^T\left[P\phi(x) + \overline{\phi(x)}\right] + \gamma C^T[P\phi(x) + \overline{\phi(x)}]$$

$$C^T\phi(x) = -\delta[0.9999 + A^T\left[P\phi(x) + \overline{\phi(x)}\right] + \beta[C^T[P\phi(x) + \overline{\phi(x)}\right] - d.$$

Collocate the above three equations by the following collocation points, $x_i = \frac{2i-1}{2N}$, $i = 1, 2, 3, \ldots, N$, where N represents the size of the matrix. Then, we get a system containing 3N algebraic equations and solve these equations by the Newtons–Raphson method that yields Hermite wavelet unknown coefficient values. Then, substitute these unknown coefficient values in (6), (8), and (10); we get the corresponding Hermite wavelet-based numerical solutions.

3.2. Hermite Wavelets Method for Fractional COVID-19 Pandemic Model

Assume that

$$S' = A^T\phi(x),\ E' = B^T\phi(x),\ I' = C^T\phi(x),\ Q' = D^T\phi(x),\ R' = F^T\phi(x). \tag{11}$$

Integrate the equations in (11) concerning x, limit from 0 to x, along with the initial conditions in (2).

$$\left.\begin{aligned} S &= 153 + A^T\left[P\varphi(x) + \overline{\varphi(x)}\right] \\ E &= 55 + B^T\left[P\varphi(x) + \overline{\varphi(x)}\right] \\ I &= 79 + C^T\left[P\varphi(x) + \overline{\varphi(x)}\right] \\ Q &= 68 + D^T\left[P\varphi(x) + \overline{\varphi(x)}\right] \\ R &= 20 + F^T\left[P\varphi(x) + \overline{\varphi(x)}\right] \end{aligned}\right\} \tag{12}$$

Now, differentiate (12) fractionally concerning x using the Caputo derivative definition; then, we get

$$\left.\begin{array}{l} {}_0^cD_x^\delta S = {}_0^cD_x^\delta\left(153 + A^T\left[P\varphi(x) + \overline{\varphi(x)}\right]\right) \\ {}_0^cD_x^\delta E = {}_0^cD_x^\delta\left(55 + B^T\left[P\varphi(x) + \overline{\varphi(x)}\right]\right) \\ {}_0^cD_x^\delta I = {}_0^cD_x^\delta\left(79 + C^T\left[P\varphi(x) + \overline{\varphi(x)}\right]\right) \\ {}_0^cD_x^\delta Q = {}_0^cD_x^\delta\left(68 + D^T\left[P\varphi(x) + \overline{\varphi(x)}\right]\right) \\ {}_0^cD_x^\delta R = {}_0^cD_x^\delta\left(20 + F^T\left[P\varphi(x) + \overline{\varphi(x)}\right]\right) \end{array}\right\}. \quad (13)$$

Substitute (13) and (12) in (2) and collocate the obtained equations by the following collocation points, $x_i = \frac{2i-1}{2N}$, $i = 1, 2, 3, \ldots, N$, where N represents the size of the matrix. Then, we get a system containing 5N nonlinear algebraic equations and solve these equations by the Newtons–Raphson method that yields the Hermite wavelet unknown coefficients' values. Then, substitute these unknown coefficient values in (12), and we get the corresponding Hermite wavelet-based fractional numerical solutions.

4. Applications of the Proposed Method

This section discusses the given system by assuming different values for the sleep factor, tension, food rate, death rate, and medicine term. We solve this system using the Hermite wavelet method, and the results are compared with the numerical method. Tables 1–3 show the different values of the $T(x), F(x)$, and $M(x)$ in the interval [0,2] in which fixed initial values have been taken for all three cases. The numerical calculations have been achieved by using the HWM.

Example 1. *Here, we solved Equation (1) by the Hermite wavelet method. Figures 1–3 represent the tension, food, and medicine on varying food intake. Table 1 justifies the numerical values by HWM with the R–K method at the constant values as follows:* $\alpha = 0.1,\ \beta = 0.2, \delta = 0.3, \gamma = 0.4, d = 0.5,$ *with initial conditions* $T(0) = 0.9999,\ F(0) = 0.0001, M(0) = 0$. *In model (1), the negative sign indicates a smaller amount. Figure 1 shows that too little food consumption affects the nervous digestive system that leads to increased tension. Figure 2 shows that continuing the consumption process of too little food leads to other complications to the body; this automatically increases medicine consumption. Figure 3 shows the effect of* α *on food. Table 2 justifies the numerical values by HWM with the R–K method at the constant values as follows,* $\alpha = -1, \beta = 0.2, \delta = 1, \gamma = 0.4, d = 0.1,$ *with same initial conditions. Tension is directly affected by sleep; when tension increases, it causes a decrease in sleep. So, Figure 4 reflects that the sleep factor is inversely proportional to the tension. Tension increases while the tension factor* δ *increases; this can be seen in Figure 5. When tension increases automatically, to control the high tension, medicines are preferred. The consumption of medicine is directly proportional to the tension that reflects Figure 6. Table 3 justifies the numerical values by HWM with the R–K method at the constant values as follows:* $\alpha = 2, \beta = 0.2, \delta = 2, \gamma = 0.4, d = 0.01,$ *with the same initial conditions. Figure 7 shows that increasing the recovery factor leads to decreasing the consumption of medicine. Any disease that causes more death for such disease consumption of medicine is also increased. The death rate and medicine consumption due to the nervous digestive system increase simultaneously, as shown in Figure 8.*

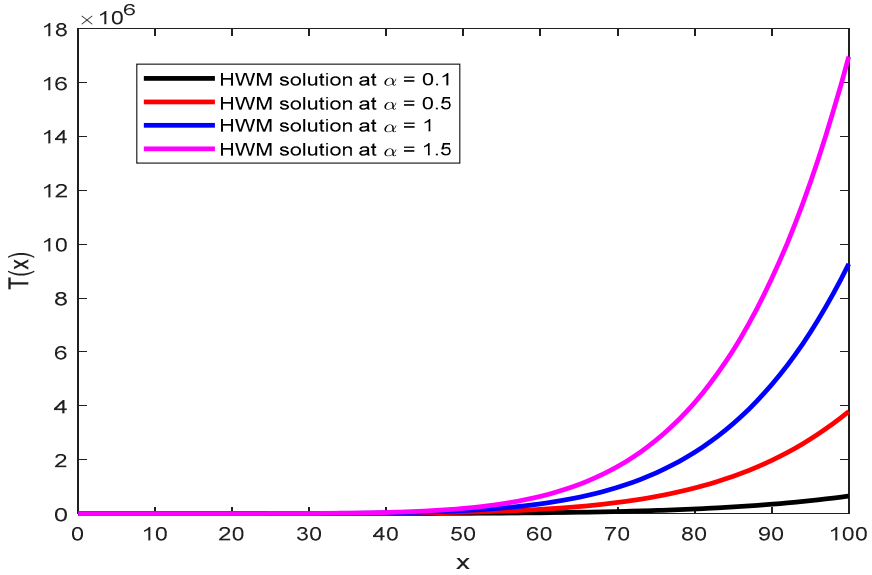

Figure 1. Influence of α on tension when $\beta = 0.2, \delta = 0.3, \gamma = 0.4, d = 0.5$.

Table 1. Numerical comparison of HWM at $\alpha = 0.1, \beta = 0.2, \delta = 0.3, \gamma = 0.4, d = 0.5$ with numerical results.

x	HWM	Numerical Result	HWM	Numerical Result	HWM	Numerical Result
	$T(x)$	$T(x)$	$F(x)$	$F(x)$	$M(x)$	$M(x)$
0.0	0.9999	0.9999	0.0001	0.0001	0.0000	0
0.1	0.9798	0.9799	0.0282	0.0282	−0.0805	−0.0804
0.2	0.9593	0.9595	0.0524	0.0525	−0.1620	−0.1618
0.3	0.9387	0.9390	0.0728	0.0729	−0.2445	−0.2442
0.4	0.9179	0.9183	0.0892	0.0893	−0.3281	−0.3277
0.5	0.8969	0.8974	0.1016	0.1018	−0.4127	−0.4122
0.6	0.8759	0.8765	0.1100	0.1103	−0.4985	−0.4979
0.7	0.8548	0.8555	0.1142	0.1147	−0.5852	−0.5845
0.8	0.8336	0.8344	0.1144	0.1150	−0.6732	−0.6724
0.9	0.8125	0.8134	0.1104	0.1112	−0.7622	−0.7613
1.0	0.7914	0.7924	0.1022	0.1032	−0.8524	−0.8514
1.1	0.7705	0.7716	0.0897	0.0909	−0.9438	−0.9427
1.2	0.7496	0.7508	0.0729	0.0743	−1.0364	−1.0352
1.3	0.7290	0.7303	0.0517	0.0534	−1.1302	−1.1289
1.4	0.7086	0.7100	0.0262	0.0281	−1.2254	−1.2240
1.5	0.6885	0.6900	−0.0038	−0.0015	−1.3218	−1.3203
1.6	0.6687	0.6703	−0.0383	−0.0357	−1.4195	−1.4179
1.7	0.6493	0.6510	−0.0773	−0.0744	−1.5187	−1.5170
1.8	0.6303	0.6321	−0.1208	−0.1176	−1.6193	−1.6175
1.9	0.6117	0.6136	−0.1690	−0.1654	−1.7213	−1.7194
2.0	0.5937	0.5957	−0.2218	−0.2178	−1.8248	−1.8228

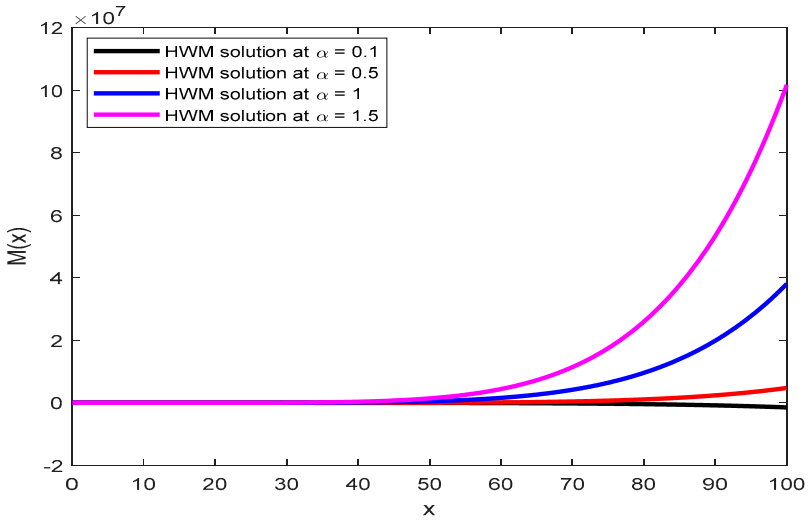

Figure 2. Influence of α on medicine when $\beta = 0.2, \delta = 0.3, \gamma = 0.4, d = 0.5$.

Table 2. Numerical comparison of HWM at $\alpha = -1, \beta = 0.2, \delta = 1, \gamma = 0.4, d = 0.1$ with numerical results.

x	HWM	Numerical Result	HWM	Numerical Result	HWM	Numerical Result
	$T(x)$	$T(x)$	$F(x)$	$F(x)$	$M(x)$	$M(x)$
0.0	0.9999	0.9999	0.0001	0.0001	0.0000	0
0.1	0.9849	0.9849	0.0985	0.0984	−0.0401	−0.0401
0.2	0.9795	0.9795	0.1942	0.1941	−0.0808	−0.0808
0.3	0.9836	0.9837	0.2882	0.2882	−0.1222	−0.1222
0.4	0.9971	0.9973	0.3814	0.3815	−0.1648	−0.1646
0.5	1.0199	1.0202	0.4747	0.4749	−0.2088	−0.2085
0.6	1.0521	1.0525	0.5690	0.5693	−0.2545	−0.2541
0.7	1.0938	1.0943	0.6651	0.6655	−0.3022	−0.3017
0.8	1.1452	1.1458	0.7639	0.7644	−0.3523	−0.3516
0.9	1.2067	1.2075	0.8662	0.8670	−0.4051	−0.4043
1.0	1.2786	1.2796	0.9731	0.9740	−0.4610	−0.4600
1.1	1.3615	1.3627	1.0854	1.0865	−0.5204	−0.5192
1.2	1.4559	1.4573	1.2041	1.2054	−0.5837	−0.5822
1.3	1.5625	1.5642	1.3302	1.3318	−0.6512	−0.6495
1.4	1.6822	1.6842	1.4648	1.4667	−0.7236	−0.7216
1.5	1.8158	1.8181	1.6091	1.6112	−0.8013	−0.7990
1.6	1.9644	1.9670	1.7641	1.7666	−0.8847	−0.8822
1.7	2.1291	2.1320	1.9313	1.9341	−0.9746	−0.9717
1.8	2.3112	2.3145	2.1119	2.1150	−1.0715	−1.0683
1.9	2.5122	2.5158	2.3074	2.3109	−1.1761	−1.1725
2.0	2.7335	2.7375	2.5192	2.5232	−1.2890	−1.2850

Table 3. Numerical comparison of HWM at $\alpha = 2, \beta = 0.2, \delta = 2, \gamma = 0.4, d = 0.01$ with numerical results.

x	HWM	Numerical Result	HWM	Numerical Result	HWM	Numerical Result
	$T(x)$	$T(x)$	$F(x)$	$F(x)$	$M(x)$	$M(x)$
0.0	0.9999	0.9999	0.0001	0.0001	0	0
0.1	0.9601	0.9602	0.1961	0.1960	−0.0308	−0.0307
0.2	0.8823	0.8825	0.3792	0.3790	−0.0605	−0.0603
0.3	0.7698	0.7701	0.5419	0.5416	−0.0878	−0.0875
0.4	0.6273	0.6277	0.6781	0.6777	−0.1118	−0.1114
0.5	0.4607	0.4612	0.7824	0.7819	−0.1316	−0.1311
0.6	0.2768	0.2774	0.8508	0.8502	−0.1465	−0.1459
0.7	0.0829	0.0836	0.8808	0.8801	−0.1560	−0.1553
0.8	−0.1129	−0.1121	0.8714	0.8706	−0.1597	−0.1589
0.9	−0.3030	−0.3021	0.8233	0.8224	−0.1576	−0.1567
1.0	−0.4798	−0.4788	0.7385	0.7375	−0.1499	−0.1489
1.1	−0.6364	−0.6353	0.6208	0.6197	−0.1370	−0.1359
1.2	−0.7670	−0.7658	0.4751	0.4739	−0.1195	−0.1183
1.3	-0.8674	−0.8661	0.3075	0.3062	−0.0982	−0.0969
1.4	−0.9351	−0.9337	0.1249	0.1235	−0.0741	−0.0727
1.5	−0.9700	−0.9685	−0.0652	−0.0667	−0.0484	−0.0469
1.6	−0.9751	−0.9735	−0.2549	−0.2565	−0.0222	−0.0206
1.7	−0.9565	−0.9548	−0.4369	−0.4386	0.0033	0.0050
1.8	−0.9244	−0.9226	−0.6043	−0.6061	0.0269	0.0287
1.9	−0.8934	−0.8915	−0.7516	−0.7535	0.0474	0.0493
2.0	−0.8831	−0.8811	−0.8752	−0.8772	0.0640	0.0660

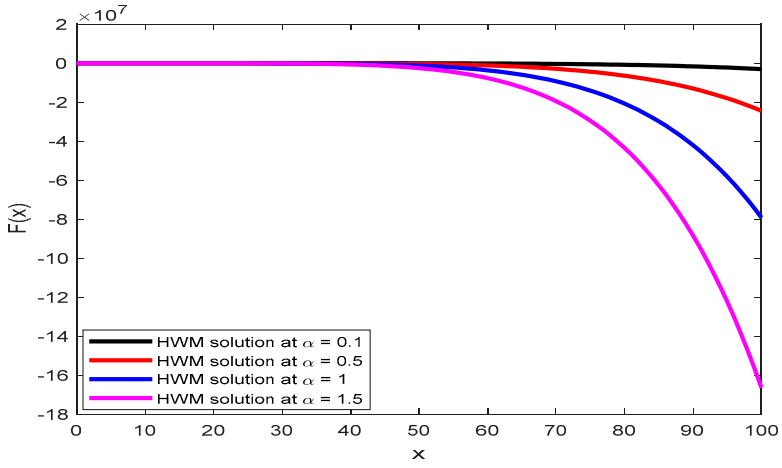

Figure 3. Influence of α on food when $\beta = 0.2, \delta = 0.3, \gamma = 0.4, d = 0.5$.

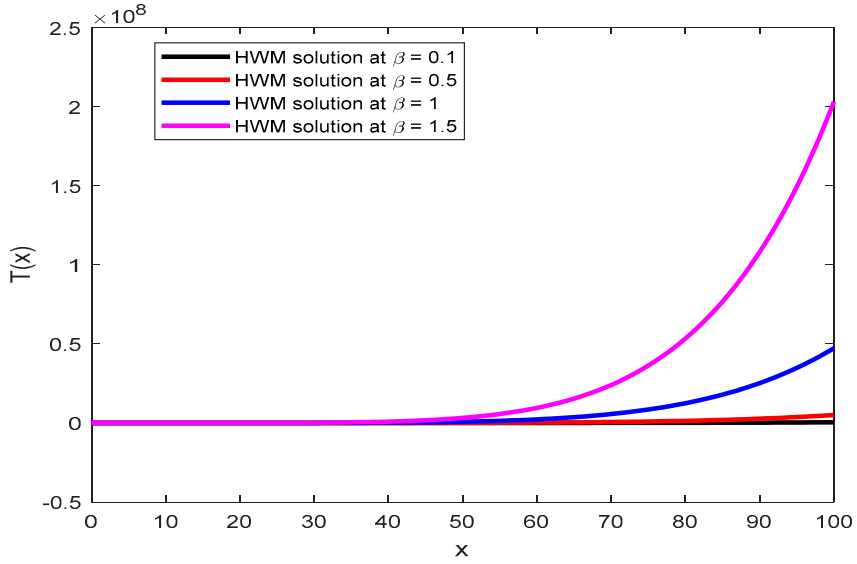

Figure 4. Influence of β on tension when $\alpha = 0.1, \delta = 0.3, \gamma = 0.4, d = 0.5$.

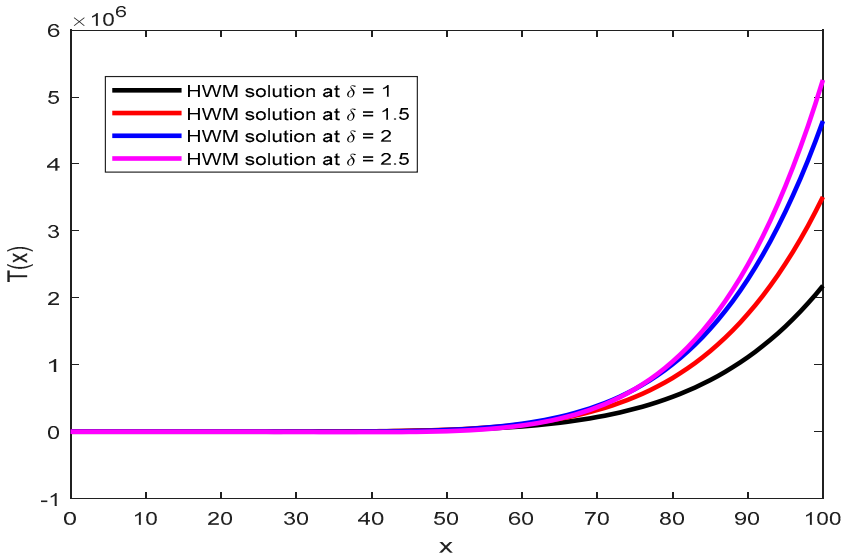

Figure 5. Influence of δ on tension when $\alpha = 0.1, \beta = 0.2, \gamma = 0.4, d = 0.5$.

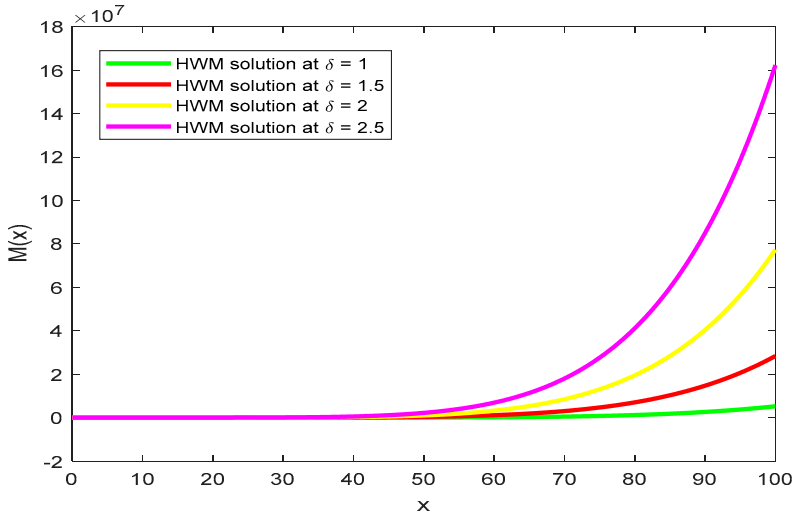

Figure 6. Influence of δ on medicine when $\alpha = 0.1, \beta = 0.2, \gamma = 0.4, d = 0.5$.

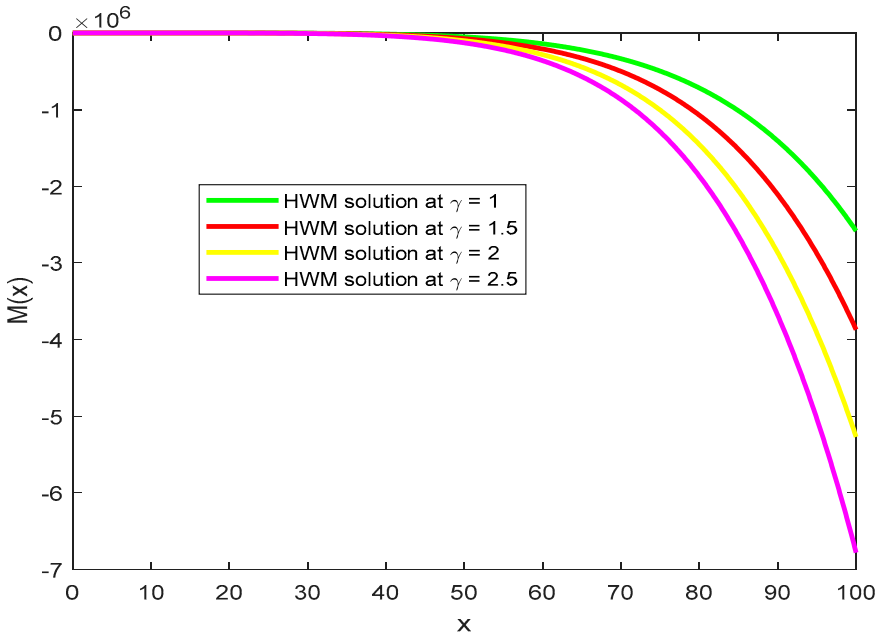

Figure 7. Influence of γ on medicine when $\alpha = 0.1, \beta = 0.2,\ \delta = 0.2, d = 0.5$.

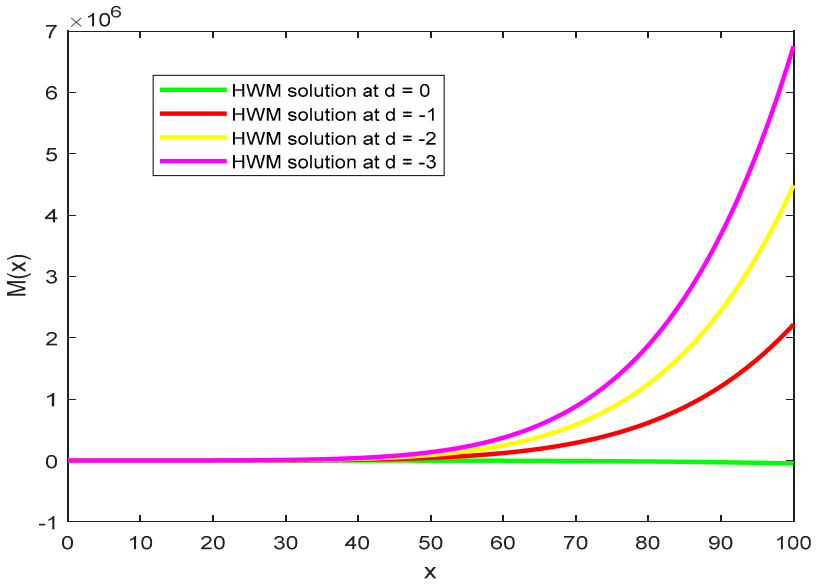

Figure 8. Influence of d on medicine when $\alpha = 0.1, \beta = 0.2,\ \delta = 0.2, \gamma = 0.4$.

Example 2. *Consider a fractional ordered COVID-19 pandemic model given in the Equation (2). Here, we solved this model by using HWM with following parameter values are as follows,* $\Lambda = 0.145$; $\mu = 0.000411$; $\beta = 0.00038$; $\pi = 0.00211$; $\gamma = 0.0021$; $\sigma = 0.0169$; $\theta = 0.0181$, *with total population* $N = 375$. *Obtained results are compared with R–K method through graphs (9–13). Figures 9–13 reflects the HWM solution at* $\delta = 1, 0.9, 0.8, 0.7$ *for the Susceptible, Exposed, Infected, Isolated, and Recovered population.*

5. Results and Discussion

From Figures 1, 3, 5 and 7, it can be observed that as the tension rate increases simultaneously, Medication also increases, which leads to the stomach's upset. Consumption of too little (too much) food also impacts the nervous-digestive system. The death rate is decreasing by increasing the consumption of Medicine. Also, from Figure 1, too little food consumption causes the high secretion of digestive juice that disturbs the stomach. The mathematical Equation (2) represents the COVID-19 pandemic model with isolated classes

in fractional order. A system of fractional-order differential equations describes this model includes the following factors, susceptible, exposed, infected, isolated, and recovered. The construction and analysis of the model (2) help us understand the mechanism of the transmission and the characteristics of diseases. Therefore, we can propose effective strategies to predict, prevent, and restrain diseases (COVID-19) and protect population health. In this model, the exposed and infected population is linked to the susceptible population. Also, we assume that the natural death rate includes the disease death rate. If there is no disease symptom, the exposed class moves with a specific rate to the isolated class, but it moves to the infected class when symptoms are developed. In Figures 9–13, we plot numerical solutions of the model (2) obtained by the HWM and the R–K method when N = 375 for α = 1, 0.9, 0.8, 0.7. From these figures, the results obtained using the HWM algorithm match the results of the R–K method well, which implies that the presented method can predict the behavior of these variables accurately in the region under consideration. The increasing number of days susceptible populations decrease, as shown in Figure 9, because the susceptible population gets exposed and infected. Figure 13 shows that when a susceptible population gets more infected, the death rate increases linearly. Figure 12 shows that when a susceptible population gets more infected, the home quarantine of the population also increases. The susceptible population decreases on increasing exposed population it can be seen in Figure 11.

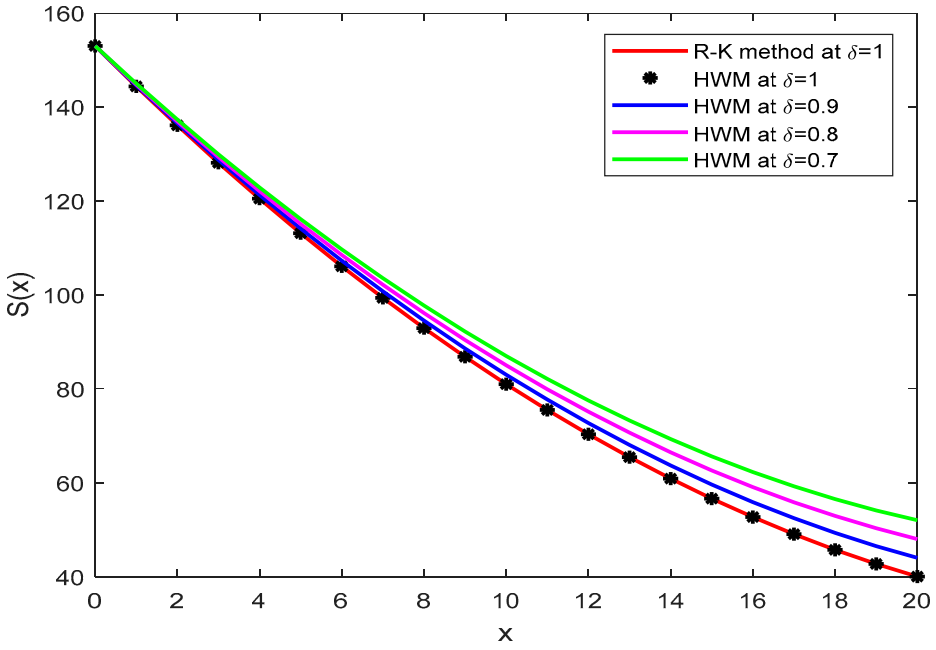

Figure 9. Graphical representation of the susceptible population at different values of δ by HWM and the R–K method.

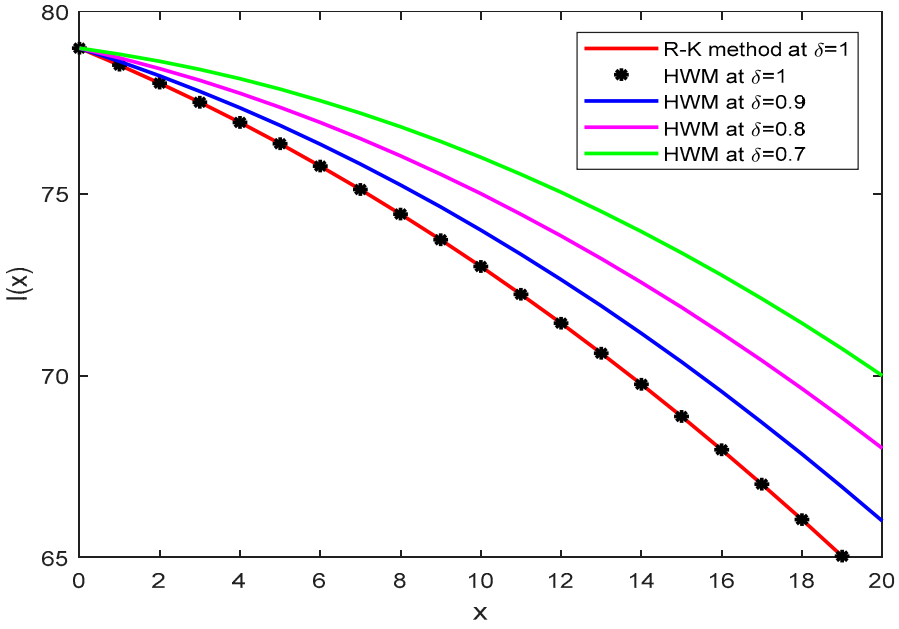

Figure 10. Graphical representation of infected population at different values of δ by HWM and the R–K method.

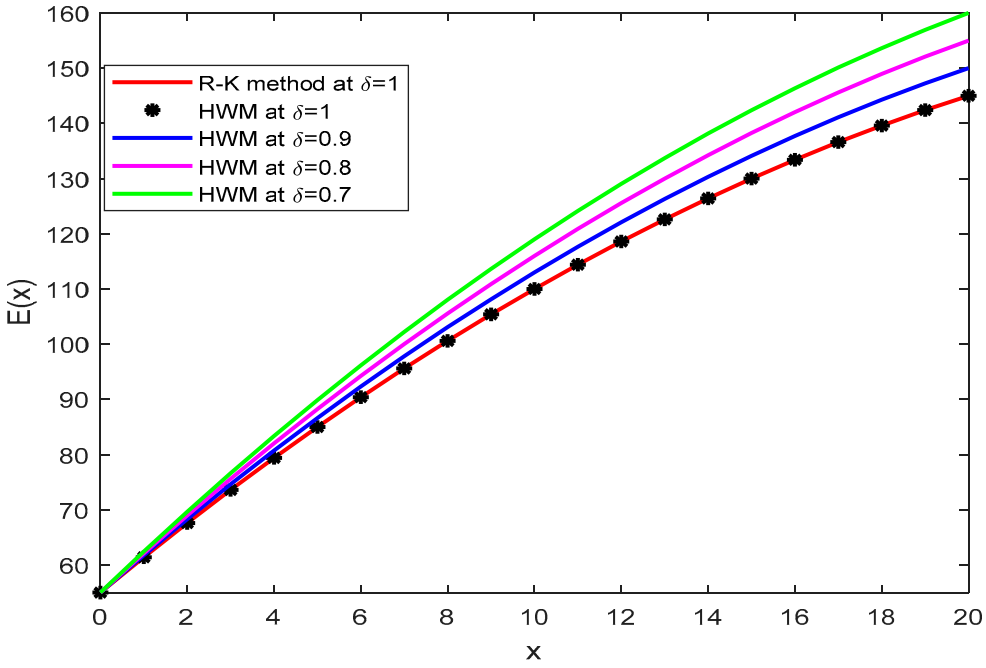

Figure 11. Graphical representation of the exposed population at different values of δ by HWM and the R–K method.

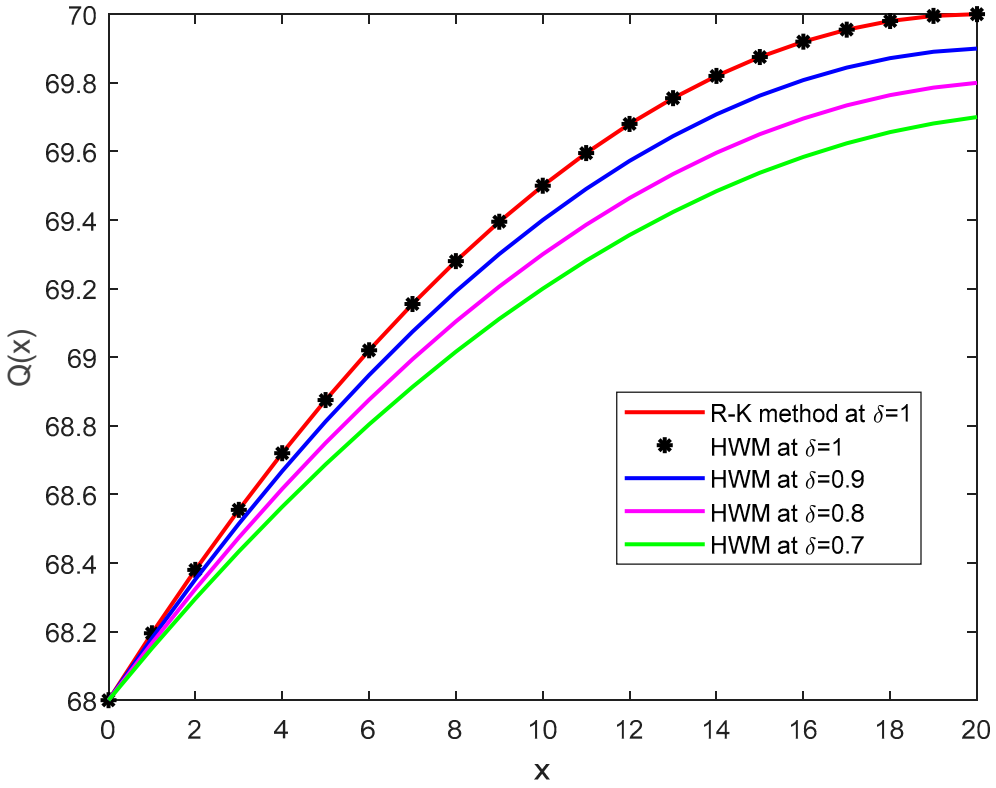

Figure 12. Graphical representation of the isolated population at different values of δ by HWM and the R–K method.

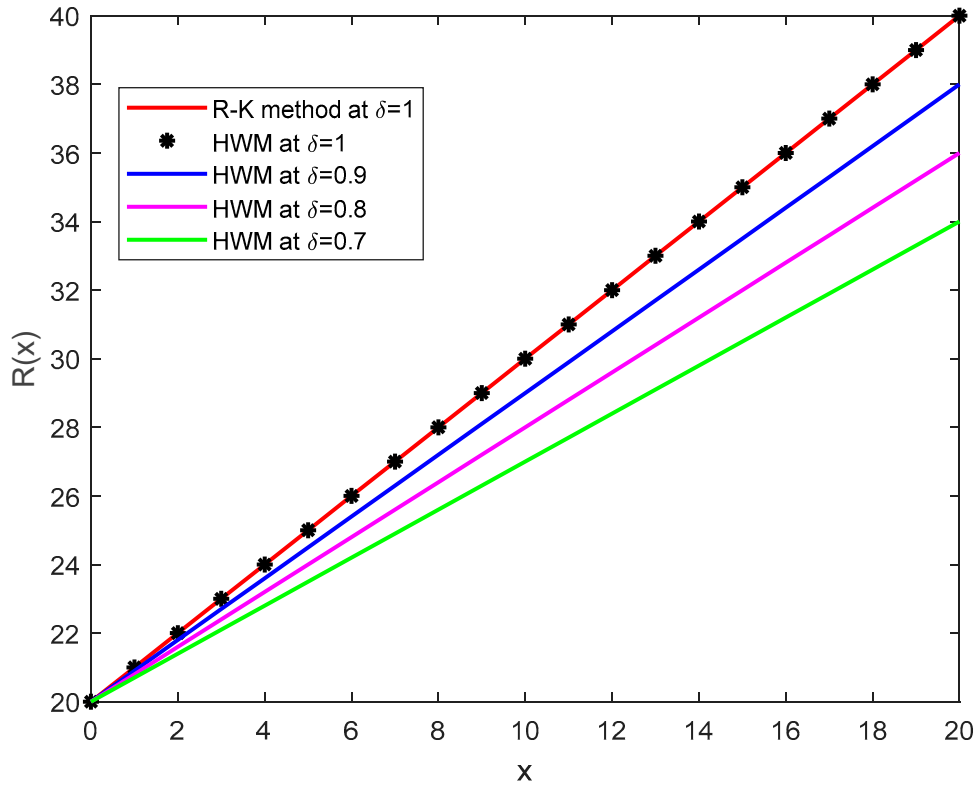

Figure 13. Graphical representation of the recovered population at different values of δ by HWM and the R–K method.

6. Conclusions

This paper has successfully applied the HWM to the digestive model, which is assumed for sleep, tension, food, and death rates. We have also observed the results numerically in detail. Analysis of this model has been shown through figures. Moreover, we have introduced the numerical values in the tables. From the tables, it may be concluded that approximate numerical results are very close to the numerical solutions (R–K method) of the governing model. It is also used to comment that these results are very close the symmetrical wave simulations of the governing model of Equation (1). Thus, considered problems are introduced to test the proposed method's efficiency, accuracy, and validity in symmetrical aspect. Also, Figures 1–8 reveals that how these parameters impact the digestive system.

Secondly, we observed one another model described by a fractional-order differential equation system with different terms: susceptible, exposed, infected, isolated, and recovered in the population. We have applied the HWM and Runge–Kutta method to simulate the proposed model. Moreover, it can also be presented that this method may also be applied for obtaining numerical solutions of the other differential equation arising in health problems in extracting features of the governing models. The method used in this paper helps to predict, prevent, and restrain diseases (COVID-19) and protect population health. Figures 9–13 reveal how the susceptible, exposed, infected, isolated, and recovered populations in symmetrical sense are interrelated.

Author Contributions: Conceptualization, Y.G.S.; formal analysis, H.M.B.; investigation and writing—original draft preparation, K.S. All authors have read and agreed to the published version of the manuscript.

Funding: This paper has been partially founded by Ministerio de Ciencia, Innovación y Universidades (No. PGC2018-097198-B-I00) and Fundación Séneca de la Región de Murcia (No. 20783/PI/18).

Institutional Review Board Statement: Not applicable.

Informed Consent Statement: Not applicable.

Data Availability Statement: The data is available from the corresponding author with a reasonable request.

Conflicts of Interest: The authors declare no conflict of interest.

References

1. Yousefi, S.A. Legendre wavelet method for solving differential equations of Lane–Emden type. *Appl. Math. Comput.* **2006**, *181*, 1417–1422. [CrossRef]
2. Verma, A.K.; Rawani, M.K.; Cattani, C. A numerical scheme for a class of generalized Burgers' equation based on Haar wavelet nonstandard finite difference method. *Appl. Numer. Math.* **2021**, *168*, 41–54. [CrossRef]
3. Hosseininia, M.; Heydari, M.H.; Cattani, C. A wavelet method for nonlinear variable-order time fractional 2D Schrödinger equation. *Discret. Contin. Dynam. Systems-S* **2021**, *14*, 2273–2295. [CrossRef]
4. Shiralashetti, S.C.; Kumbinarasaiah, S. Theoretical study on continuous polynomial wavelet bases through wavelet 288 series collocation method for nonlinear lane-Emden type equations. *Appl. Math. Comput.* **2017**, *315*, 591–602.
5. Shiralashetti, S.C.; Kumbinarasaiah, S. Laguerre wavelets collocation method for the numerical solution of the Benjamina–Bona–Mohany equations. *J. Taibah Univ. Sci.* **2019**, *13*, 9–15. [CrossRef]
6. Agarwal, P.; Singh, R.; Rehman, A. Numerical solution of a hybrid mathematical model of dengue transmission with relapse and memory via Adam–Bashforth–Moulton predictor-corrector scheme. *Chaos Solitons Fractals* **2021**, *143*, 110564. [CrossRef]
7. Sánchez, Y.J.; Sabir, Z.; Günerhan, H.; Baskonus, H.M. Analytical and approximate solutions of design of a novel biological nervous stomach mathematical model. *Discret. Dynam. Nat. Soc.* **2020**, *2020*, 9.
8. Praveen, A.; Ram, S. Modelling of transmission dynamics of Nipah virus (Niv): A fractional-order Approach. *Phys. A Stat. Mech. Appl.* **2020**, *547*, 124243.
9. Günay, B.; Agarwal, P.; Guirao, J.L.G.; Momani, S. A Fractional Approach to a Computational Eco-Epidemiological Model with Holling Type-II Functional Response. *Symmetry* **2021**, *13*, 1159. [CrossRef]
10. Attiqul, R.; Ram, S.; Praveen, A. Modeling, analysis, and prediction of new variants of COVID-19 and dengueco-infection on complex network. *Chaos Solitons Fractals* **2021**, *150*, 111008.

11. Goyal, M.; Baskonus, H.M.; Prakash, A. Regarding new positive, bounded, and convergent numerical solution of nonlinear time-fractional HIV/AIDS transmission model. *Chaos Solitons Fractals* **2020**, *139*, 110096. [CrossRef]
12. Yel, G.; Akturk, T. A New Approach to (3+1) Dimensional Boiti–Leon–Manna–Pempinelli Equation. *Appl. Math. Nonlinear Sci.* **2020**, *5*, 309–316. [CrossRef]
13. Gao, W.; Veeresha, P.; Prakasha, D.G.; Baskonus, H.M.; Yel, G. New approach for the model describing the deathly disease in pregnant women using Mittag Leffler function. *Chaos Solitons Fractals* **2020**, *134*, 109696. [CrossRef]
14. Singh, J.; Kumar, D.; Hammouch, Z.; Atangana, A. A fractional epidemiological model for computer viruses pertaining to a new fractional derivative. *Appl. Math. Comput.* **2018**, *316*, 504–515. [CrossRef]
15. Kumbinarasaiah, S.; Rezazadeh, H. Numerical solution for the fractional-order one-dimensional telegraph equation via wavelet technique. *Int. J. Nonlinear Sci. Numer. Simul.* **2020**, *22*, 767–780.
16. Zhang, Z.; Zeb, A.; Egbelowo, O.F.; Vedat, S.E. Dynamics of a fractional-order mathematical model for COVID-19 epidemic. *Adv. Differ. Equ.* **2020**, *420*, 1–11. [CrossRef] [PubMed]
17. Vladimirov, V.S. *Equations of Mathematical Physics*; Marcel Dekker Incorporated: New York, NY, USA, 1971.
18. Gupta, A.K.; Saha Ray, S. An investigation with Hermite Wavelets for accurate solution of Fractional Jaulent–Miodek equation associated with energy-dependent Schrödinger potential. *Appl. Math. Comput.* **2015**, *270*, 458–471. [CrossRef]
19. Shiralashetti, S.C.; Kumbinarasaiah, S. New generalized operational matrix of integration to solve nonlinear singular boundary value problems using Hermite wavelets. *Arab J. Basic Appl. Sci.* **2019**, *26*, 2591–2600. [CrossRef]
20. Lanbaran, N.M.; Celik, E.; Yigider, M. Evaluation of Investment Opportunities with Interval-Valued Fuzzy Topsis Method. *Appl. Math. Nonlinear Sci.* **2020**, *5*, 461–474. [CrossRef]
21. Ihan, E.; Kiymaz, I.O. A generalization of truncated M-fractional derivative and applications to fractional differential equations. *Appl. Math. Nonlinear Sci.* **2020**, *5*, 171–188.
22. Durur, H.; Yokus, A. Exact solutions of (2+1)-Ablowitz-Kaup-Newell-Segur equation. *Appl. Math. Nonlinear Sci.* 2021. [CrossRef]
23. Li, Y.M.; Rashid, S.; Hammouch, Z.; Baleanu, D.; Chu, Y.M. New Newton's Type Estimates Pertaining to Local Fractional Integral via Generalized p-Convexity with Applications. *Fractals* **2021**, *29*, 2140018-747. [CrossRef]
24. Aksoy, N.Y. The Solvability of First Type Boundary Value Problem for a Schrödinger Equation. *Appl. Math. Nonlinear Sci.* **2020**, *5*, 211–220. [CrossRef]